Continental weathering following a Cryogenian glaciation: evidence from calcium and magnesium isotopes

Simone A. Kasemann[1*], Philip A.E. Pogge von Strandmann[2], Anthony R. Prave[3], Anthony E. Fallick[4], Tim Elliott[5], Karl-Heinz Hoffmann[6]

[1] Department of Geosciences and MARUM-Center for Marine Environmental Sciences, University of Bremen, 28334 Bremen, Germany

* Corresponding author; Phone +49 (0)421-218-65930; e-mail: skasemann@marum.de

[2] Institute of Earth and Planetary Sciences, UCL and Birkbeck, University of London, Gower Street, London, WC1E 6BT, UK, p.strandmann@ucl.ac.uk

[3] Earth Sciences, University of St Andrews, St Andrews KY16 9AL, UK, ap13@st-andrews.ac.uk

[4] Scottish Universities Environmental Research Centre, East Kilbride G75 OQF, UK, t.fallick@suerc.gla.ac.uk

[5] Department of Earth Sciences, University of Bristol, Bristol BS8 1RJ, UK, Tim.Elliott@bristol.ac.uk

[6] Geological Survey of Namibia, P.O. Box 2168, Windhoek, Namibia, khhoffmann@mme.gov.na

Abstract

A marked ocean acidification event and elevated atmospheric carbon dioxide concentrations following the extreme environmental conditions of the younger Cryogenian glaciation has been inferred from boron isotope measurements. Calcium and magnesium isotope analyses offer additional insights into the processes occurring during this time. Data from Neoproterozoic sections in Namibia indicate that following the end of glaciation the continental weathering flux transitioned from being of mixed carbonate and silicate character to a silicate-dominated one. Combined with the effects of primary dolomite formation in the

cap dolostones, this caused the ocean to depart from a state of acidification and return to higher pH after climatic amelioration. Differences in the magnitude of stratigraphic isotopic changes across the continental margin of the southern Congo craton shelf point to local influences modifying and amplifying the global signal, which need to be considered in order to avoid overestimation of the worldwide chemical weathering flux.

Keywords: calcium isotopes, magnesium isotopes, continental weathering, cap carbonates, Neoproterozoic

1 Introduction

The response of the Earth system to recent changes in forcing parameters has attracted much attention. The response to and recovery from a hypothesised ultra-greenhouse state following the global glaciations of the Neoproterozoic represent one of the most acute tests of feedbacks within the Earth system to maintain an equable environment. Such events are marked geologically by deposition worldwide of 'cap carbonate' (Hoffman and Schrag, 2002), a distinctive rock layer that directly overlies glacial deposits or glaciated surfaces (Hoffman and Schrag, 2002; James et al., 2001; Kennedy, 1996; Kennedy et al., 1998, 2001a, 2001b; Williams, 1979).

Although cap carbonates are recognised as a fingerprint of the icehouse-to-greenhouse transition (Hoffman et al., 1998), no consensus exists as to their causal mechanism or the atmospheric-oceanic conditions under which they formed. A widely held view is that elevated atmospheric CO_2 would have generated extreme greenhouse conditions, acidified the post-glacial ocean, increased surface temperatures and precipitation and, as a consequence, continental weathering and riverine transport. This in turn led to enhanced rock (silicate) weathering thereby augmenting CO_2 consumption, increasing ocean alkalinity and pH, and, ultimately, lowering temperatures.

Stratigraphic trends in the stable isotope compositions of the cap carbonates are distinctive and largely consistent with the model described above. Carbon isotopes initially

display a sharp negative excursion followed by recovery to more positive values. Even though lively debate remains regarding the exact cause of this excursion, many studies have shown the overall isotopic trends to be stratigraphically systematic and of global significance (e.g. Halverson et al., 2005). Further, concomitant negative boron isotope excursions in post-glacial carbonates have been used in a recent approach to address ocean pH fluctuations during the transition from icehouse to greenhouse states (Kasemann et al., 2010).

Having reconstructed ocean pH conditions for the older and younger Cryogenian pan-glacial states and identified a temporary ocean acidification event for the younger interglacial (Kasemann et al., 2010), this study deals with the next critical step in deciphering Cryogenian environmental conditions: to resolve the discrepancy between having an acidic ocean whilst maintaining relatively high rates of carbonate sedimentation, and how the Earth system recovered from the extreme ocean pH conditions. The combined application of calcium and magnesium isotopes provides unique insight into the evolution of continental weathering, ocean alkalinity, and carbonate sedimentation under these unusual conditions.

1.1 Background

Chemical weathering of continental silicates consumes atmospheric CO_2, and acts as a climate-moderating process (e.g. Kump et al., 2000). In addition, weathering delivers carbonate and metal ions to the oceans (Berner et al., 1983, 1990; Kump et al., 2000; Walker et al., 1981) where they are removed via precipitation of calcium carbonate with implications for ocean alkalinity (Archer et al., 2000; Dessert et al., 2003; Gaillardet et al., 1999). Calcium and magnesium are key components in both chemical weathering reactions (e.g. Berner et al., 1983, 1990; Kump et al., 2000; Walker et al., 1981) and carbonate precipitation. In seawater and carbonates, their isotope ratios can change in response to large flux imbalances, fluctuations in ocean temperature, variations in mineralogy and rates of precipitation (e.g. Blättler et al., 2011; De La Rocha and DePaolo, 2000; Li et al., 2012; Pogge von Strandmann, 2008; Shen et al., 2009; Teng et al., 2008; Tipper et al., 2006a, 2006b; Zhu and Macdougall, 1998). Importantly, calcium and magnesium isotope ratios in

ancient carbonates are strongly rock-buffered, hence largely unaffected by diagenesis (Fantle and DePaolo, 2007).

Ca and Mg have long modern oceanic residence times of ca. 1 Myr and 10 Myr, respectively (e.g. Berner and Berner, 1996; Holland, 1978). Accordingly, Ca and Mg isotopes preserved in Neoproterozoic interglacial carbonates can be used to trace and potentially quantify changes in continental weathering and ocean alkalinity and, consequently, yield insights into Earth's ancient climatic states. However, the isotope composition of seawater may still change over shorter time intervals if the influence of the driving factor is large enough and/or seawater exchange within the depositional basin is restricted (Holmden et al., 2012).

To test this, we have measured Ca and Mg isotope ratios on samples from carbonate units of the Neoproterozoic Otavi Group in NW Namibia (Fig. 1; Kasemann et al., 2005, 2010). These sections were deposited on the low-latitude continental margin of the southern Congo craton, represent different depositional facies (foreslope and platform) and contain a record of the younger Cryogenian (ca. 635 Ma) pan-glacial to greenhouse transition. The combined stable isotopic datasets for these sections enable us to construct and combine weathering/alkalinity, palaeo-pH and carbon chemistry profiles over a variety of water depths and settings for one depositional basin. Further, we can assess if Ca and Mg isotopes can be used: (i) as stratigraphic fingerprints recording characteristic trends specific to the younger Cryogenian (Marinoan) glaciation-deglaciation sequence; (ii) to identify their regional (local) and/or global significance; and (iii) to evaluate the nature and scale of chemical weathering and Earth system recovery during the Cryogenian climatic extremes.

2 Material and methods

2.1 Samples

Samples selected for this study were collected from the Neoproterozoic Otavi Group in NW Namibia (see Supplemental Online Material), and are the same samples on which Kasemann et al. (2005, 2010) previously obtained and reported C, O, and B isotope ratios

(Supplementary Online Material). The sampled sections were from two well-exposed areas (Fig. 1), the eastern Kaokoveld carbonate platform (Ombaatjie and Khowarib sections) and the Fransfontein Ridge shelf-slope break (Fransfontein section), and define a transect from shallow- to deeper-marine settings across the palaeocontinental margin of the Congo craton (Kasemann et al., 2010). In addition, the sections capture the meltback phase of the younger Cryogenian (ca. 635 Ma) Ghaub Formation and the return to more moderate climatic conditions (Halverson et al., 2005; Hoffmann et al., 2004).

As noted in Kasemann et al. (2005, 2010), the sample localities have not experienced any degree of metamorphism and are only moderately deformed with broad and open folds. The rocks selected for isotope analyses preserve exquisite evidence of original depositional features and structures, are uniform and micritic in texture, and contain no observed evidence of secondary alteration or recrystallization. Prior to isotope analyses, the quality of the samples was checked by scanning electron microscope (SEM) and trace element analyses using secondary ionisation mass spectrometry (SIMS), as detailed in Kasemann et al. (2005, 2010).

2.2 Analytical techniques

Calcium isotope ratios were determined in the laboratories of the Bristol Isotope Group (BIG) using the preparation technique, measurement routine and data collection method detailed in Kasemann et al. (2005, 2008) and Supplemental Online Material. Analyses were performed on a Thermo Finnigan Triton thermal ionisation mass spectrometer. Ca isotope ratios are given relative to NIST SRM 915a in the conventional $\delta^{44/40}$Ca (‰) notation. The $n(^{44}Ca)/n(^{40}Ca)$ ratio of the reference material for each analytical session was reproduced to within 0.1‰ (2σ), with an internal uncertainty of about 0.05‰ ($2\sigma_{mean}$). The uncertainty (2σ) on the isotope ratio of the samples is about 0.15‰.

Magnesium isotope ratios $n(^{26}Mg)/n(^{24}Mg)$ were measured using a Thermo Finnigan Neptune multicollector ICP-MS at Bristol University using an Elemental Scientific Inc. Apex-Q introduction system. Samples were analysed in a sample-standard bracketing technique,

relative to the standard DSM-3 (Galy et al., 2003). Analyses and purification chemistry were performed as detailed in Pogge von Strandmann (2008) and Pogge von Strandmann et al. (2011). The external uncertainty (2σ) of the analyses is ±0.05‰ on δ^{26}Mg, as determined by repeated analyses of the same seawater sample (n = 14; chemistry = 14) (Foster et al., 2010) (see Supplemental Online Material for further details)

3 Results

The isotopic data are summarised in Fig. 2 (and Supplementary Online material; for detailed discussion of the C, O and B isotopic data see Kasemann et al., 2005, 2010). $\delta^{44/40}$Ca values for Fransfontein (foreslope; Figs. 2, 3) display a sinusoidal profile starting at 1.1‰ in the Keilberg cap-dolostone, decline to 0.8‰ in Maieberg dolostone, climb to 1.3‰ in limestone and end at 0.9‰ in the Elandshoek dolostones. The Ombaatjie (mostly inner-mid platform to peritidal settings) $\delta^{44/40}$Ca profile is bow-shaped and starts with a value of 1.1‰ in the cap dolostone, declines to 0.4‰ in the overlying deeper-marine rhythmites of the Maieberg limestone and returns steadily to 1.1‰ through the shallowing-upward trend of the inner-mid platform to peritidal Maieberg dolostones (Kasemann et al., 2005). In stark contrast, the $\delta^{44/40}$Ca values for the nearby Khowarib section (similar palaeoenvironmental setting as the Ombaatjie section) show relatively constant but rather low values (average of 0.51 ± 0.14‰, 1σ) with non-systematic scatter from 0.2 to 0.7‰ through the entire profile of 15 samples (Figs. 2, 3).

δ^{26}Mg profiles were constructed for the Keilberg-Maieberg cap-carbonate sequence at Fransfontein and Ombaatjie. In the former, δ^{26}Mg starts in the cap at -1.6‰, rises to -1.4‰ and declines through the Maieberg Formation to ca. -2.1‰ (Figs. 2, 3). In the latter, δ^{26}Mg starts at -1.8‰, increases to -1.4‰, then declines to -2.1‰ in Maieberg limestones before rising gradually to -1.5‰ through the rest of the formation.

The Ca and Mg isotope inflections and trends do not correspond to or coincide with facies changes or lithostratigraphically defined formational boundaries. Consequently, the Ca

and Mg isotope variation is not lithology-dependent nor does it reflect diagenetic alteration. Thus, we interpret the isotopic data as recording original seawater signals. This is not unexpected in that Ca and Mg are major elements in carbonate rocks but not usually in post-depositional fluids, and so their isotopic compositions are buffered against diagenetic change (Fantle and DePaolo, 2007; Silva-Tamayo et al., 2010a).

4 Discussions

4.1 Calcium isotope signals: local, regional or global?

Changes in the calcium isotope composition of seawater depend primarily on the net imbalance between calcium delivery to the ocean and burial in sediments as the flux of calcium increases/decreases in response to continental weathering and erosion (De La Rocha and DePaolo, 2000; Fantle and DePaolo, 2005; Zhu and Macdougall, 1998). Kasemann et al. (2005) documented a negative Ca isotope excursion of about 0.8‰ in the mostly shallow platform carbonate rocks (Ombaatje section) in Namibia and interpreted that as reflecting a temporary imbalance between Ca input from continental weathering and Ca precipitation following the younger Cryogenian glacial. Subsequently, Silva-Tamayo et al. (2010b) obtained Ca isotope profiles for broadly equivalent successions in central-W Brazil and NW Canada (Fig. 4). They compared the isotopic pattern preserved in inner and outer platform carbonates from Brazil and Canada to the isotopic shallow platform pattern (Ombaatjie section) from Namibia and concluded that the Ca isotope perturbations were global and stratigraphically unique, and thus could be employed as a chemostratigraphic correlation tool. Examination of our Namibian data indicates otherwise: we find non-trivial differences in the Ca isotope variation across the palaeocontinental margin represented by the early Ediacaran Keilber-Maieberg Formation of the Otavi Group (Fig. 4).

Focussing solely on the well-constrained Keilberg-Maeiberg cap-carbonate sequences those at Fransfontein (which record a foreslope setting) and Ombaatjie (shallow platform setting) display what could be viewed uncritically as comparable, bow-shaped $\delta^{44/40}$Ca profiles (Fig. 4). However, even though both begin at ca. 1.1‰, smoothly decline,

and then rise back to values of ca. 1‰, the nadir is significantly lower at Ombaatjie (ca. 0.4‰) than at Fransfontein (ca. 0.8‰). This reveals a statistically significant ($\alpha = 0.05$) difference in relative isotopic variation (at least 0.4‰) between the two localities. Further, the Ca isotope profile at Khowarib (a shallow marine platform section similar to Ombaatjie) shows data scattering non-systematically around 0.5‰. Thus, there is substantial and statistically significant variability in $\delta^{44/40}$Ca data along a single shallow platform-to-slope transect (mean $\delta^{44/40}$Ca ± measure of dispersion 1σ; Fransfontein: 1.01 ± 0.15‰, Ombaatjie: 0.86 ± 0.24‰, Khowarib: 0.51 ± 0.14‰), which refutes the claim by Silva-Tamayo et al. (2010b) that $\delta^{4/404}$Ca profiles are globally reproducible.

The observed differences in the $\delta^{44/40}$Ca profiles for the Namibian transect suggest a regional influence amplifying the global pattern. Especially, the considerably different and non-systematic pattern for the shallow platform Khowarib section reveals the potential of a strong local control on the $\delta^{44/40}$Ca profile. Because the Fransfontein section would have been located along the edge of an ocean-facing continental margin, and given the consistency of that section's $\delta^{44/40}$Ca data, we consider this profile to be the most reliable record of global ocean conditions. This, then, indicates that the extreme Ca isotope values (as low as 0.1‰ to as high as 2‰; Fig. 4) observed in the shallow marine sections from Brazil, Canada (Silva-Tamayo et al., 2010b) and Namibia (Kasemann et al., 2005), are signals recording local modifications, and show that the temporary global shift of ~0.5‰ in the Fransfontein section (from 0.8‰ to 1.3‰) can be magnified to as much as 2‰ (Fig. 4). Consequently, our results counsel prudence before applying Ca isotope stratigraphy as a tool to correlate Neoproterozoic postglacial carbonate successions, and question the reliability of $\delta^{44/40}$Ca profiles to differentiate between the interglacial successions. In addition, while investigating global Ca mass balance evolution and weathering flux predictions, care has to be taken in choosing a $\delta^{44/40}$Ca pattern that is minimally influenced by local factors.

4.2 Calcium and magnesium isotope signals: environmental implications

223 The local control on the $\delta^{44/40}Ca$ pattern does, however, provide a unique opportunity to
224 improve our understanding of, and ability to reconstruct, the environmental conditions
225 associated with extreme Neoproterozoic climatic changes. Factors that could have
226 influenced the Ca isotope composition of the Neoproterozoic oceans, apart from changes in
227 the continental weathering flux (and regime), include the rate of carbonate precipitation as
228 well as mineralogy (e.g. calcite/aragonite), and ocean temperature and pH (Fig. 5). Hence,
229 considering the scenarios proposed for the formation of cap carbonates, the Ca isotope
230 composition of carbonate precipitates would certainly change:
231
232 *(i) Alkalinity and temperature changes*
233 It has been proposed that cap carbonates owe their origin to upwelling of deep basinal
234 alkaline water during deglaciation (Grotzinger and Knoll, 1995; Ridgwell et al., 2003).
235 Another view is that Cryogenian surface ocean temperature increased from -1.5°C to 30°C
236 (Higgins and Schrag, 2003; Pierrehumbert, 2004) during deglaciation. In the former scenario,
237 stimulation of carbonate precipitation would involve an increased Ca output and, hence, a
238 positive Ca isotope excursion. In the latter, since Ca isotope fractionation decreases with
239 increasing temperature (Gussone et al., 2005; Marriott et al., 2004; Nägler et al., 2000), the
240 temperature effect should also drive a positive Ca isotope shift of ~ 0.6‰ (Gussone et al.,
241 2005) during cap carbonate precipitation, because carbonate is ubiquitously isotopically
242 lighter than the Ca ion in aqueous solution. In contrast, our $\delta^{44/40}Ca$ data show a declining,
243 rather than increasing, trend.
244
245 *(ii) Precipitation rate changes*
246 Alternatively, experimental studies on spontaneous calcite precipitation have demonstrated
247 that Ca isotope fractionation values between calcite and aqueous Ca ($\Delta^{44/40}Ca_{calcite\text{-}aqueous}$) are
248 positively correlated (i.e. increase) with the precipitation rate, although the effect becomes
249 weaker with increasing temperature (Tang et al., 2008). This positive rate-dependence on
250 the Ca isotope fractionation is, especially at high precipitation rates, counterbalanced by the

negative temperature-dependence and thus would not be able to produce the smooth and temporary declining isotope trend. Instead, it could only explain the non-systematic scatter and low $\delta^{44/40}$Ca of the shallow-marine Khowarib section marked by a thick Keilberg-Maieberg carbonate sequence (Figs. 2, 3).

(iii) Changes induced by mineralogy

Since aragonite has a Ca isotope ratio 0.6‰ lower than cogenetic calcite (Gussone et al., 2005), a global shift in carbonate mineralogy from calcite to aragonite is capable of producing the negative Ca isotope excursion observed in the Cryogenian successions. Such a scenario would require dominantly calcite mineralogy at the start of the deglaciation followed by principal aragonite precipitation up-section in the Keilberg-Maieberg, where the return to more positive values would document the initiation of a new global ocean steady state with a higher seawater Ca isotope composition (or, if it is temporary, a shift back to dominant calcite mineralogy). However, the sedimentary record and the lithology-independent Ca isotope variations do not support this. So far, a systematic study on Ca isotope fractionation in dolomite has not been published and insufficient Ca isotope data on dolomites have been reported (Holmden, 2009; Kasemann et al., 2005; Steuber and Buhl, 2006) to assess if a shift from potentially primary dolomite at the start of cap deposition to calcite and/or aragonite is capable of producing the Ca isotope excursion. Then again, such a shift is not supported by the lithology-independent Ca isotope variation.

(iv) Changes induced by variation in pH and continental weathering

A temporary acidification scenario during which carbonate deposition decreases due to ocean acidification and subsequently increases due to weathering feedbacks (Payne et al., 2010) would result in an initial decrease in the carbonate depositional flux, accompanied by Ca accumulation in the seawater and a decrease in the Ca isotope composition, followed by an increase in carbonate deposition and return to a steady state and higher Ca isotope values. Boron isotope data obtained from the same samples offer support to such a scenario:

279 Kasemann et al. (2010) modelled a marked ocean acidification event compatible with
280 elevated postglacial pCO_2 concentration for the younger deglaciation period. However, due
281 to the limited amount of seafloor carbonate, carbonate dissolution together with a disruption
282 of carbonate precipitation would by itself not be capable of producing the observed negative
283 isotope excursion (Blättler et al., 2011). During the Phanerozoic, a change in composition of
284 weathered lithology could change the Ca isotope composition of seawater when, for
285 example, Ca isotope fractionation in marine shelled organisms drives carbonate rocks to
286 more negative values compared to the average igneous rock ($\delta^{44/40}$Ca ~0.9‰, see DePaolo,
287 2004 and references therein). However, Neoproterozoic carbonate rocks do not contain
288 marine shelled organisms and the $\delta^{44/40}$Ca values (e.g. $\delta^{44/40}$Ca ~1‰, Ombaatjie and
289 Fransfontein Fms, supplementary data) are on average higher than modern oozes ($\delta^{44/40}$Ca
290 ~0.4‰) and similar to average igneous rocks (e.g. $\delta^{44/40}$Ca 1 to 1.4‰, Tipper et al., 2006a).
291 Similar to Ca, the Mg isotope composition of seawater (Fig. 5) is predominantly
292 controlled by a change in riverine Mg isotope flux (Tipper et al., 2006b), along with the ratio
293 between the two seawater sinks: hydrothermal removal (which scavenges Mg quantitatively,
294 and hence causes no isotope fractionation), and carbonate formation, which preferentially
295 takes up light ^{24}Mg, and therefore drives seawater isotopically heavier ($\Delta^{26/24}Mg_{calcite\text{-}aqueous}$ ~ -
296 2.7‰, $\Delta^{26/24}Mg_{dolomite\text{-}aqueouss}$ ~ -1.8 to -2.7‰ depending of the type of dolomite mineralisation;
297 Galy et al., 2002; Higgins and Schrag, 2010; Tipper et al., 2006b). In addition, a temporary
298 ocean acidification event could decrease the Mg isotope ratio while a parallel rise in
299 temperature would again drive an increase in δ^{26}Mg during cap carbonate precipitation
300 (observed for carbonates precipitated under laboratory conditions; Li et al., 2012). On the
301 other hand, δ^{26}Mg values in seawater are more dependent on the dominant type of
302 weathering rock, i.e. silicates versus carbonates, and preliminary studies in modern
303 weathering environments indicate further significant isotope fractionation between mineral
304 residue and solution (e.g. Pogge von Strandmann et al., 2008) potentially generated via
305 silicate soil formation (Pogge von Strandmann et al., 2012; Tipper et al., 2006b, 2010) and
306 biological productivity in soils or rivers (Black et al., 2006; Bolou-Bi et al., 2010). Silicate

307 rocks from the continental crust display $\delta^{26}Mg$ values ranging from -0.5 to +0.9‰ (Li et al.,
308 2010; Liu et al., 2010; Shen et al., 2009; Tipper et al., 2006b), while Cryogenian carbonate
309 rocks tend to be lower ($\delta^{26}Mg$ between -2.2 and -1.1‰) with an average Mg isotopic
310 composition ~-1.6‰, similar to reported Phanerozoic ($\delta^{26}Mg$: −4.4 to −1‰, Tipper et al.,
311 2006b) and Ediacaran carbonate data ($\delta^{26}Mg$: -2.3 to -0.8‰, Pokrovsky et al., 2011).
312 Focussing on a temporary imbalance between weathering influx and precipitation as
313 the main driver for both isotope excursions, continental weathering in the greenhouse
314 aftermath of a glaciation would not only drive enhanced weathering of silicates but also of
315 carbonates. While carbonate weathering does not sequester CO_2 on geological timescales,
316 its alkalinity flux might account for the deposition of the postglacial cap carbonates (Higgins
317 and Schrag, 2003; Hoffman and Schrag, 2002). It has been recognised that alkalinity release
318 from silicate weathering was neither rapid enough nor sufficient to account for cap
319 carbonates; also, that the dissolution of carbonate minerals would be enhanced during
320 deglaciation (lower temperature and emerged platforms) (Le Hire et al., 2009; Higgins and
321 Schrag, 2003; Hoffman and Schrag, 2002) while maximum silicate weathering is reached
322 after cap carbonate deposition (following melting and transgression) (Kasemann et al., 2005;
323 Nogueria et al., 2007).
324 The assumed change from carbonate-dominated to silicate-dominated weathering is
325 apparent in the relationship and timing of the Ca and Mg isotope pattern for the Ombaatjie
326 platform section. Both $\delta^{44/40}Ca$ and $\delta^{26}Mg$ display a bow-shaped negative shift indicating the
327 temporary elevated weathering flux. However, the Mg excursion starts and terminates first
328 with the nadir at the transition between the Keilberg cap dolostones and Maieberg
329 limestones, whereas the nadir in the Ca excursion occurs stratigraphically higher (Fig. 2) and
330 above where aragonite fan pseudomorphs are locally preserved. Consequently, the
331 termination of cap dolostone sedimentation does not mark the end of enhanced weathering
332 (Kennedy et al., 2001b), but may reflect the change from carbonate-dominated (low $\delta^{26}Mg$)
333 to silicate-dominated (low $\delta^{44/40}Ca$) weathering as carbonate platforms are drowned by rising
334 sea level (Hoffman and Schrag, 2002).

That continental weathering is indeed the principal driver for the Ca and Mg isotope variation is also implied by the distinctive relationship between C, Ca, and Mg isotopes, in particular in the Ombaatjie section (Fig. 6). It is remarkable that for the Keilberg-Maieberg Formation, with the consistent exception of the contact sample (OBTJ 43) between the glacial and the Keilberg sequence (see also discussion of Fig. 2 in Kasemann et al., 2005), there are robust relationships between the carbon isotopic composition of the carbonates and the corresponding Ca and Mg isotope ratios (Fig. 6). The trends are plausibly linear: for $\delta^{44/40}Ca$ versus $\delta^{13}C_{carb}$, r = 0.79, >99% significant for n = 10 (Fig. 6a); for $\delta^{26}Mg$ versus $\delta^{13}C_{carb}$, r = 0.82, >99% significant for n = 9 (Fig. 6b). This strongly suggests that Ca, Mg and C isotopes are coupled through continental (silicate + carbon-bearing rocks) weathering. As mentioned above, silicate weathering draws down CO_2 but carbonate weathering does not remove CO_2 from the atmosphere in the long term, permitting at least partial decoupling of some of the C isotope excursion from the recovery to more normal atmospheric CO_2 levels. In the interpretation of Fig. 6 it is crucial to remember that the negative $\delta^{13}C_{carb}$ excursions during the Neoproterozoic are considered global and representative of "primary perturbation of the surface carbon cycle" with a "characteristic timescale of 10^5 to 10^6 years" (Johnston et al., 2012). Explanations invoking isotope resetting during diagenesis, or a massive pool of dissolved (or, indeed, particulate) organic carbon, have been convincingly ruled out by these authors. Thus, moving from $\delta^{13}C_{carb}$ close to zero to values of -6‰ or less likely implies an Earth system shifting between two end-member modes of operation. The first is similar to that of today with a balance between delivery of carbon to the ocean and sequestration of carbon in sediments at a ratio of carbonate C to organic C of 4 to 1. The second is where there is an enhanced input to the ocean of isotopically light carbon, presumed by Johnston et al. (2012) to be either methane or ancient organic matter in sediments delivered by weathering.

The first end-member mode would be characterised by carbonate $\delta^{44/40}Ca > 1.2‰$ (and perhaps as high as ~1.4‰), and $\delta^{26}Mg > -1.4‰$ (and perhaps ~ -1.0‰). The second mode, by contrast, has $\delta^{44/40}Ca \leq 0.4‰$ and $\delta^{26}Mg \leq -2.1‰$ (Fig. 6d). We note that these

363 latter values are not inconsistent with an enhanced riverine contribution from weathering of
364 organic-rich sedimentary lithologies. Within this general scenario, the relationships illustrated
365 in Fig. 6 then reflect various stages of the Earth system intermediate between the two end
366 members, with the proviso that absolute values of $\delta^{44/40}$Ca and δ^{26}Mg are subject to
367 modification by the processes already discussed above. The straight lines in Fig. 6 then
368 represent, in a certain sense, the locus of mixing ratios (or transitions between end member
369 modes of operation): note that we do not claim to have described (or measured) actual end
370 members, only transitions towards them. The linearity is explained by relatively constant
371 proportions of C : Ca : Mg in the ocean input, and the deviations of individual points from
372 strict linearity may reflect various processes, including short-term differences in the input
373 terms (e.g. decoupling of input sources), modification of isotope ratios by other processes as
374 described above, and buffering of isotope ratio changes for the various elements depending
375 on the different oceanic residence times. Such 'noise' may be elucidated by consideration of
376 $\delta^{44/40}$Ca versus δ^{26}Mg. High δ^{26}Mg is always accompanied by high $\delta^{44/40}$Ca at times of low
377 continental weathering, and low δ^{26}Mg is always accompanied by low $\delta^{44/40}$Ca at times of
378 enhanced continental weathering. However, high $\delta^{44/40}$Ca is not always accompanied by high
379 δ^{26}Mg, and intermediate δ^{26}Mg can have high or low $\delta^{44/40}$Ca perhaps signifying the changing
380 influence of carbonate weathering (Fig. 6d).
381
382 **4.3 Modelling seawater calcium and magnesium isotope excursions**
383 To test the extent to which the postulated changes in the continental weathering input and
384 regime (i.e. episodes dominated by carbonate and silicate) are capable of producing the
385 observed Ca and Mg isotope excursions, and also to elucidate timing and magnitude, we use
386 a series of dynamic box models. The oceanic box models were calculated assuming that the
387 sources of Ca to the oceans are continental weathering and hydrothermal fluids, and the sole
388 source of Mg is continental weathering (in accordance with mass balance models for the
389 Phanerozoic, e.g. Blättler et al., 2011; Payne et al., 2010; Pogge von Strandmann et al.,
390 2013). The common sink of Ca and Mg is net carbonate burial, while Mg is additionally

removed via hydrothermal activity (which scavenges Mg quantitatively, and hence causes no isotope fractionation), and dolomite formation (high Mg sink compared to calcite). Both the calcium and magnesium cycles are modelled by taking the isotope ratios and magnitudes of the fluxes and isotope fractionation factors between sinks and sources from modern mass balance estimates (see Blättler et al., 2011; Tipper et al., 2006b and references therein) (Fig. 7). For the calcium mass balance equation the hydrothermal flux was set to 2.0×10^{12} mol yr^{-1} with $\delta^{44/40}Ca = 0.9‰$, the basic river flux to 2.3×10^{13} mol yr^{-1} with an initial $\delta^{44/40}Ca$ of 1.0‰ to adjust for initial steady state conditions, and the initial oceanic calcium reservoir was set to 1.4×10^{19} mol; $\Delta^{44/40}Ca_{carbonate\text{-}aqueous} = -0.8‰$. The mass balance equation for the magnesium model takes account of 5.6×10^{12} mol yr^{-1} basic river flux with an initial $\delta^{26}Mg$ of -1.0‰ and an initial oceanic magnesium reservoir of 7.3×10^{19} mol. Magnesium removal by carbonate precipitation is taken to be constant at -2.7‰ (equal to $\Delta^{26/24}Mg_{calcite\text{-}aqueous}$), and hence independent of the mineralogy of carbonate output (i.e. we do not assume different fractionation factors for dolomite or limestone precipitation; Higgins and Schrag, 2010). This accounts for the observed broad range in $\delta^{26}Mg$ caused by the type of dolomite mineralisation and the facies-independent isotope pattern. The sink for both isotope systems is calculated as a partition coefficient, i.e. it is responsive to the seawater concentration. In the model, both elemental cycles are linked through the common riverine flux sources, carbonate and silicate rocks. The oceanic Mg and Ca isotope ratio then evolves as the balance of the carbonate and silicate mixture of the younger interglacial surface runoff changes through time. Bearing in mind the different element abundances of the two main lithologies, the average end-member silicate flux is taken as having $\delta^{44/40}Ca \sim 1.2‰$ and $\delta^{26}Mg \sim -0.3‰$, whereas the average end-member carbonate flux has $\delta^{44/40}Ca \sim 0.8‰$ and $\delta^{26}Mg \sim -2.5‰$ (Tipper et al. 2006a,b).

Initially, the steady-state balance of the system was perturbed by changing the continental source flux linked to the assumed change from carbonate- to silicate-dominated weathering. The Ca isotope excursion observed on the slope (Fransfontein section), and considered to be the most reliable record of global ocean conditions, can be best matched by

419 a combined (50% each) carbonate plus silicate weathering flux of 9x (all fluxes are given as
420 a multiplier of the present day flux; see Holland, (2005)) for about 500 kyr, followed by a
421 dominant silicate weathering pulse of 6x for 1 Myr. In contrast, an initial, 500 kyr-lasting
422 carbonate plus silicate weathering flux of 20x, followed by a dominant silicate weathering
423 pulse of 15x for 1 Ma would be necessary to produce the Ca isotope excursion observed on
424 the platform (Ombaatjie section) (Fig. 8a,b). The inferred twofold increase in weathering
425 fluxes emphasizes the magnified global shift in the local platform signal as a result of a
426 restricted (embayed) basin or water body size rather than actually higher fluxes.
427 Furthermore, to produce the initial $\delta^{26}Mg$ increase right at the base of the cap and to fully
428 decouple the Ca and Mg isotope excursion we would have to assume high primary dolomite
429 formation for the first e.g. 100 kyr (cap dolostone, 85% Mg sink: Keilberg is primary dolomite,
430 i.e. was a large Mg sink at the time of deposition) followed by primary carbonate (calcite
431 and/or aragonite) precipitation (present day 15 – 28% Mg sink; Holland, 2005; Tipper et al.,
432 2006b). Alternatively, an exclusive silicate weathering influx of e.g. 20x for 1 Myr would also
433 produce the general isotope pattern observed on the platform, but in contrast to what we
434 observe in the isotope record, the nadir in $\delta^{44/40}Ca$ would occur earlier than the one in $\delta^{26}Mg$
435 (Fig. 8c). A much lower silicate weathering influx of e.g. 5x for 1 Myr, would still be capable of
436 reproducing the Ca isotope pattern on the slope but would not be sufficient to generate a
437 significant Mg pattern (Fig 8d). Note, that we have ignored the potential effects of changing
438 temperature and mineralogy in order to investigate the effects of weathering alone.
439 In an attempt to infer CO_2 consumption during increased silicate weathering in the
440 post-panglacial environment, we use the calculated river fluxes from the oceanic box model.
441 Our simplistic calculation is based on the assumption that, as in modern rivers, silicate
442 weathering rate and CO_2 consumption rate stay linear (Gaillardet et al., 1999). A CO_2
443 consumption of 6.9×10^{19} mol in 1.5 Myr is inferred by applying the modern ratio of silicate
444 weathering flux (Ca and Mg) and CO_2 consumption fluxes on the modelled silicate
445 weathering flux from Fransfontein (silicate weathering increases post-snowball to 4.5x, then
446 6x). This is a ~5-fold increase in silicate weathering compared to the “normal” modern rate of

447 $8.7x10^{12}$ mol C yr^{-1} lasting for about 1.5 Myr (only continental weathering; Gaillardet et al.,
448 1999).
449 Beside the discussion on rock (silicate) weathering augmenting CO_2 consumption and
450 controlling ocean pH in the younger Cryogenian glacial aftermath, the timescale and rate of
451 'cap carbonate' precipitation is a matter of on-going debate (e.g. Hoffman et al., 2007). In our
452 model we found that a time period of at least 3 Myr is needed to drive the entire Ca-Mg
453 isotope perturbation on both the slope and platform Keilberg-Maieberg carbonate sections,
454 assuming modern ocean residence times for Ca and Mg. This time period is in excellent
455 agreement with a model calculation on Ca isotope oscillation in Brazilian cap carbonates
456 (Silva-Tamayo et al., 2010b) and U–Pb ages from China (Condon et al., 2005). Focussing on
457 the postglacial Keilberg cap dolostones, our model predicts a deposition period of ~100 kyr
458 and a sedimentation rate between 0.15 to 0.2 mm yr^{-1} for Keilberg cap dolostone going from
459 slope to platform. In addition, a uniform deposition period of ~1 Myr with an average
460 sedimentation rate ranging from 0.03 mm yr^{-1} on the slope to 0.14 and potentially up to 0.22
461 mm yr^{-1} on the platform are implied for the Maieberg limestone. However, timescale and rate
462 of deposition of Keilberg cap dolostone inferred from the model are in sharp contrast with
463 rapid deposition of <10 kyr (between 2000 and 10000 years; Higgins and Schrag, 2003;
464 Hoffman et al., 2007; Kennedy et al., 2001b) and an average sedimentation rate of 0.01 m yr
465 $^{-1}$ (3.8 to 19.0 mm yr^{-1}) as inferred by climate models (Hoffman et al., 2007) and
466 sedimentological features implying fast deposition (e.g. Hoffman, 2011). While our timescale
467 of cap dolostone deposition exceeds the duration inferred by climate models, it, however,
468 correlates with magnetostratigraphic data suggesting that cap dolostones accumulated over
469 several hundreds of thousands of years (Kilner et al., 2005; Trindade et al., 2003) implying
470 either much slower glacial meltdown, or cap dolostone accumulation surpassing the period of
471 glacio-eustatic rise (Hoffman et al., 2007). Note that our oceanic box model is not designed
472 to highly resolve the time of cap dolostone deposition but to reproduce the overall Ca-Mg
473 isotope pattern. To critically assess the geochemical evolution of the Cryogenian-Ediacaran
474 ocean-atmosphere system and to account for palaeogeography and palaeobathymetry, as

well as for other environmental conditions and feedback mechanisms, more sophisticated Earth system models are needed. In addition, to explicitly simulate and assess the changing influx and significance of continental silicate weathering (especially for the Keilberg cap dolostone deposition), additional proxy data, e.g. lithium isotopes, are needed which respond solely to silicate weathering over short timescales.

4.4 Continental weathering and ocean pH

If, as suggested by our data, the younger Cryogenian pan- to interglacial transition was indeed a time of enhanced continental weathering, then the concomitant flux of alkalinity into the seawater must have enabled the ocean to return from an acidification event to a state of pH normalcy. The linkage between enhanced continental weathering and buffered ocean pH is emphasized by the observation that the transient ocean acidification event, indicated by the negative $\delta^{11}B$ excursion of the Keilberg-Maieberg sequence (Kasemann et al., 2010), is essentially tracked by $\delta^{13}C$, $\delta^{44/40}Ca$ and $\delta^{26}Mg$ (Fig. 2) and, by implication, continental weathering. As reported in Kasemann et al. (2010), the $\delta^{11}B$-ocean pH profiles from the palaeocontinental margin are comparable in cyclicity. However, similar to the regional differences in the magnitude of the Ca and Mg isotope excursion, slight regional differences in timing of the B isotope excursion exist. In case of the shelf-slope break section (Fransfontein) - our most reliable record of global ocean conditions - the $\delta^{11}B$-ocean pH excursion is essentially tracked by $\delta^{13}C$ and $\delta^{44/40}Ca$. The recovery from the ocean acidification event starts within the Maieberg limestones and hence, in time with the change in the weathering regime and maximum silicate weathering flux, indicating the connection between ocean pH, continental weathering and potentially pCO_2 (Fig. 9). On the shallow-marine platform section (Ombaatjie), the nadir in $\delta^{11}B$-ocean pH occurs already in the Keilberg cap dolostones and well before the nadir in $\delta^{13}C$, $\delta^{44/40}Ca$ and $\delta^{26}Mg$ (Fig. 2). In fact, there is a progressive change between $\delta^{11}B$ versus $\delta^{13}C$ (see Fig. 2 in Kasemann et al., 2005), $\delta^{44/40}Ca$ and especially $\delta^{26}Mg$ (Fig. 6c). The smooth “clockwise” trend highlights different periods when either B changed and Mg did not, or Mg changed and B remained

503 constant. This difference in timing was initially interpreted as a potential disconnection
504 between ocean pH and atmospheric CO_2 (Kasemann et al., 2005) and hence weathering.
505 Instead, the early nadir in $\delta^{11}B$ and the partial decoupling from $\delta^{13}C$, $\delta^{44/40}Ca$ and $\delta^{26}Mg$ at
506 the platform could be the result of a combination of processes linked to the general change in
507 the weathering regime and the local scale of the weathering signal. Considering the
508 magnified continental weathering signal on the platform, the early nadir in $\delta^{11}B$-ocean pH
509 implies that the pH of the seawater was locally influenced by the enhanced rise in alkalinity,
510 which must have buffered the shallow and potentially restricted water body on the platform
511 first and foremost, as compared to the open ocean on the shelf-slope break. Additionally,
512 while the dominant carbonate weathering flux at the outset is able to increase alkalinity and
513 buffer pH, it would not remove CO_2 from the atmosphere in the long term.
514
515 **5 Conclusions**
516 Calcium and magnesium isotope patterns, preserved in the Otavi Group carbonate rocks
517 from Namibia, indicate an enhanced continental weathering influx following the demise of the
518 younger Cryogenian (ca. 635 Ma) glaciation. This observation is in general accordance with
519 results gained from broadly equivalent successions in Brazil and Canada by Silva-Tamayo et
520 al. (2010b), signifying a global Ca perturbation of the ocean via flux imbalances in response
521 to continental weathering. Yet, our study identifies significant differences in the magnitude of
522 the Ca isotope excursions between the different basins and notably even along the single
523 palaeocontinental margin transect of the Congo craton in Namibia. A simple oceanic box
524 model based on the Ca and Mg isotope data from Namibia revealed a twofold increase in the
525 calculated weathering flux for the platform setting compared to the slope setting. Instead of
526 implying variable weathering fluxes across the palaeocontinental margin, the more
527 pronounced platform signal (Ombaatjie section) rather suggests a local influence of a
528 restricted basin or water body, potentially amplifying the global pattern represented by the
529 slope (Fransfontein) section. The non-systematic scatter in the second platform section
530 (Khowarib) points to an additional strong local control on the Ca isotope signal due to

potential differences in rates of carbonate precipitation, carbonate supersaturation and/or temperature. Consequently, Ca isotope profiles are not globally reproducible and not a reliable chemostratigraphic correlation tool, and extreme regional isotope signals can lead to an overestimate of the global chemical weathering flux. Observed differences in the timing of the Ca and Mg isotope excursion in both of our platform and slope sections are best explained by primary dolomite formation during Keilberg cap dolostone sedimentation together with a change from carbonate- to silicate-dominated continental weathering as carbonate platforms are drowned by rising sea level. Our box model implies an initial carbonate plus silicate weathering flux and a change in the continental weathering regime above the cap dolostone sedimentation and during deposition of the deeper-water limestone rhythmites of the lower Maieberg Formation. Dominant silicate weathering is reached stratigraphically higher in the Maieberg limestones near and/or above where aragonite fans occur and in the highstand sequence (Hoffman, 2011) of the Maieberg dolostones. The enhanced continental weathering flux and concomitant flux of alkalinity into the seawater must have enabled the Earth system to recover from low ocean pH conditions and to maintain carbonate sedimentation even under acidic ocean conditions. Consequently, the documentation of combined proxy records of $\delta^{44/40}Ca$ and $\delta^{26}Mg$ with $\delta^{11}B$ and $\delta^{13}C$ allows to better delineate the response and recovery from a hypothesised postglacial, ultra-greenhouse state and how this impacts on the Earth system's capacity to maintain an equable environment.

Acknowledgments

This work was funded by a Natural Environment Research Council New Investigator Award (NE/C507529/1) to SAK. PPvS is funded by NERC Research Fellowship NE/1020571/1. We are grateful to C. Taylor for the sample preparation in the analytical facilities at Bristol University. The manuscript has benefited from careful reviews by A. Rooney and two anonymous reviewers, and editorial handling from G. Henderson.

559 **References**

560 Archer, D.E., Winguth, A., Lea, D. Mahowald, N., 2000. What caused the glacial/interglacial
561 atmospheric pCO_2 cycles? Rev. Geophys. 38, 159-189.

562 Berner, R.A., Lasaga, A.C., Garrels, R.M., 1983. The carbonate-silicate geochemical cycle
563 and its effect on atmospheric carbon-dioxide over the past 100 million years. Am. J.
564 Sci. 283, 641-683.

565 Berner, R.A.,1990. Global CO_2 degassing and the carbon-cycle - comment on Cretaceous
566 Ocean Crust at Dsdp Site-417 and Site-418 - carbon uptake from weathering vs loss
567 by magmatic outgassing. Geochim. Cosmochim. Acta 54, 2889-2890.

568 Berner, E.K., Berner, R.A., 1996. Global Environment: Water, Air and Geochemical Cycles.
569 Prentice Hall, Upper Saddle River, N.J.

570 Black, J.R., Yin, Q.Z., Casey, W.H., 2006. An experimental study of magnesium-isotope
571 fractionation in chlorophyll-a photosynthesis. Geochim. Cosmochim. Acta 70, 4072-
572 4079.

573 Blättler, C.L., Jenkyns, H.C., Reynard, L.M., Henderson, G.M., 2011. Significant increases in
574 global weathering during Oceanic Anoxic Events 1a and 2 indicated by calcium
575 isotopes. Earth Planet. Sci. Lett. 309, 77-88.

576 Bolou-Bi, E.B., Poszwa, A., Leyval, C., Vigier, N., 2010. Experimental determination of
577 magnesium isotope fractionation during higher plant growth. Geochim. Cosmochim.
578 Acta 74, 2523-2537.

579 Condon, D., Zhu, M., Bowring, S., Wang, W., Yang, A., Jin, Y., 2005. U–Pb ages from the
580 Neoproterozoic Doushantuo Formation, China. Science 308, 95-98.

581 De La Rocha, C.L., DePaolo, D.J., 2000. Isotopic evidence for variations in the marine
582 calcium cycle over the Cenozoic. Science 289, 1176-1178.

583 DePaolo, D.J., 2004. Calcium isotopic variations produced by biological, kinetic, radiogenic
584 and nucleosynthetic processes. Rev. Mineral. Geochem. 55, 255-288.

585 Dessert, C., Dupre, B., Gaillardet, J., Francois, L.M., Allegre, C.J., 2003. Basalt weathering
586 laws and the impact of basalt weathering on the global carbon cycle. Chem. Geol.
587 202, 257-273.
588 Fantle, M.S., DePaolo, D.J., 2005. Variations in the marine Ca cycle over the past 20 million
589 years. Earth Planet. Sci. Lett. 237, 102-117.
590 Fantle, M.S., DePaolo, D.J., 2007. Ca isotopes in carbonate sediment and pore fluid from
591 ODP site 807A: The Ca^{2+} (aq)-calcite equilibrium fractionation factor and calcite
592 recrystallization rates in Pleistocene sediments. Geochim. Cosmochim. Acta 71,
593 2524-2546.
594 Foster, G.L., Pogge von Strandmann, P.A.E., Rae, J.W.B., 2010. Boron and magnesium
595 isotopic composition of seawater. Geochem. Geophys. Geosyst. 11, Q08015.
596 doi:10.1029/2010GC003201.
597 Gaillardet, J., Dupré, B., Louvat, P., Allegre, C.J., 1999. Global silicate weathering and CO_2
598 consumption rates deduced from the chemistry of large rivers. Chem. Geol. 159, 3-
599 30.
600 Galy, A., Bar-Matthews, M., Halicz, L., O'Nions, R.K., 2002. Mg isotopic composition of
601 carbonate: insight from speleothem formation. Earth Planet. Sci. Lett. 201, 105-115.
602 Galy, A., Yoffe, O., Janney, P.E., Williams, R.W., Cloquet, C., Alard, O., Halicz, L., Wadwha,
603 M., Hutcheon, I.D., Ramon, E., Carignan, J., 2003. Magnesium isotope heterogeneity
604 of the isotope standard SRM 980 and new reference materials for magnesium-
605 isotope-ratio measurements. J. Anal. Atom. Spectrom. 18, 1352-1356.
606 Grotzinger, J.P., Knoll, A.H., 1995. Anomalous carbonate precipitates: is the Precambrian
607 the key to the Permian? Palaios 10, 578-596.
608 Gussone, N., Böhm, F., Eisenhauer, A., Dietzel, M., Heuser, A., Teichert, B.M.A., Reitner, J.,
609 Wörheide, G., Dullo, W.-C., 2005. Calcium isotope fractionation in calcite and
610 aragonite. Geochim. Cosmochim. Acta 69, 4485-4494.

611 Halverson, G.P., Hoffman, P.F., Schrag, D.P., Maloof, A.C. and Rice, A.H.N., 2005. Toward
612 a Neoproterozoic composite carbon-isotope record. Geol. Soc. Am. Bull. 117, 1181-
613 1207.
614 Higgins, J.A., Schrag, D.P., 2003. Aftermath of a snowball Earth: Geochem. Geophys.
615 Geosyst. 4, 1028. doi: 10.1029/2002GC000403.
616 Higgins, J.A., Schrag, D.P., 2010. Constraining magnesium cycling in marine sediments
617 using magnesium isotopes. Geochim. Cosmochim. Acta 74, 5039-5053.
618 Hoffman, P.F., Kaufman, A.J., Halverson, G.P., Schrag, D.P.A., 1998. Neoproterozoic
619 Snowball Earth. Science 281, 1342-1346.
620 Hoffman, P.F., Schrag, D.P., 2002. The snowball Earth hypothesis: testing the limits of global
621 change. Terra Nova 14, 129-155.
622 Hoffman, P.F., Halverson, G.P., Domack, E.W., Husson, J.M., Higgins, J.A., Schrag, D.P.,
623 2007. Are basal Ediacaran (635 Ma) post-glacial “cap-dolostones” diachronous?
624 Earth Planet. Sci. Lett. 258, 114-131.
625 Hoffman, P.F., 2011. Strange bedfellows: glacial diamictite and cap carbonate from the
626 Marinoan (635 Ma) glaciation in Namibia. Sedimentology 58, 57-119.
627 Hoffmann, K.H., Condon, D.J., Bowring, S.A., Crowley, J.L., 2004. U-Pb zircon date from the
628 Neoproterozoic Ghaub Formation, Namibia: Constraints on Marinoan glaciations.
629 Geology 32, 817-820.
630 Holland, H.D., 1978. The Chemistry of the Atmosphere and the Oceans. Wiley-Interscience,
631 New York.
632 Holland, H.D., 2005. Sea level, sediments and the composition of seawater. Am. J. Sci. 305,
633 220-239.
634 Holmden, C., 2009. Ca isotope study of Ordovician dolomite, limestone, and anhydrite in the
635 Williston Basin: Implications for subsurface dolomitization and local Ca cycling.
636 Chem. Geol. 268, 180-188.

637 Holmden, C., Papanastassiou, D.A., Blanchon, P., Evans, S., 2012. $\delta^{44/40}$Ca variability in
638 shallow water carbonates and the impact of submarine groundwater discharge on Ca-
639 cycling in marine environments. Geochim. Cosmochim. Acta 83, 179-194.
640 James, N.P., Narbonne, G.M., Kyser, T.K., 2001. Late Neoproterozoic cap carbonates:
641 Mackenzie Mountains, northwestern Canada: precipitation and global glacial
642 meltdown. Can. J. Earth Sci. 38, 1229-1262.
643 Johnston, D.T., Macdonald, F.A., Gill, B.C., Hoffman, P.F., Schrag, D.P., 2012. Uncovering
644 the Neoproterozoic carbon cycle. Nature 483, 320-323.
645 Kasemann, S.A., Hawkesworth, C.J., Prave, A.R., Fallick, A.E., Pearson, P.N., 2005. Boron
646 and calcium isotope composition in Neoproterozoic carbonate rocks from Namibia:
647 Evidence for extreme environmental change. Earth Planet. Sci. Lett. 231, 73-86.
648 Kasemann, S.A., Schmidt, D.N., Pearson, P.N., Hawkesworth, C.J., 2008. Biological and
649 ecological insights into Ca isotopes in planktic foraminifers as a palaeotemperature
650 proxy. Earth Planet. Sci. Lett. 271, 292-302.
651 Kasemann, S.A., Prave, A.R., Fallick, A.E., Hawkesworth, C.J., Hoffmann, K.-H., 2010.
652 Neoproterozoic ice ages, boron isotopes and ocean acidification: Implications for a
653 snowball Earth. Geology 38, 775-77.
654 Kennedy, M.J., 1996. Stratigraphy, sedimentology, and isotopic geochemistry of Australian
655 Neoproterozoic postglacial cap dolostones: deglaciation, δ^{13}C excursions, and
656 carbonate precipitation. J. Sed. Res. 66, 1050-1064.
657 Kennedy, M.J., Runnegar, B., Prave, A.R., Hoffmann, K.-H., Arthur, M.A., 1998. Two or four
658 Neoproterozoic glaciations? Geology 26, 1059-1063.
659 Kennedy, M.J., Christie-Blick, N., Prave, A.R., 2001a. Carbon isotopic composition of
660 Neoproterozoic glacial carbonates as a test of paleoceanographic models for
661 snowball Earth phenomena. Geology 29, 1135-1138.
662 Kennedy, M.J., Christie-Blick, N., Sohl, L.E., 2001b. Are Proterozoic cap carbonates and
663 isotopic excursions a record of gas hydrate destabilization following Earth's coldest
664 intervals? Geology 29, 443-446.

665 Kilner, B., MacNiocaill, C., Brasier, M., 2005. Low-latitude glaciation in the Neoproterozoic of
666 Oman. Geology 33, 413-416.
667 Kump, L.R., Brantley, S.L., Arthur, M.A., 2000. Chemical weathering, atmospheric CO_2 and
668 climate. Annu. Rev. Earth Planet. Sci. 28, 611-667.
669 Le Hir, G., Donnadieu, Y., Goddéris, Y., Pierrehumbert, R.T., Halverson, G.P., Macouin, M.,
670 Nédélec, A., Ramstein, G., 2009. The snowball Earth aftermath: Exploring the limits
671 of continental weathering processes. Earth Planet. Sci. Lett. 277, 453-463.
672 Li, W.-Y.,Teng, F.-Z., Ke, S., Rudnick, R.L., Gao, S., Wu, F.-Y., Chappell, B.W., 2010.
673 Heterogeneous magnesium isotopic composition of the upper continental crust.
674 Geochim. Cosmochim. Acta 74, 6867-6884.
675 Li, W., Chakraborty, S., Beard, B.L., Romanek, C.S., Johnson, C.M., 2012. Magnesium
676 isotope fractionation during precipitation of inorganic calcite under laboratory
677 conditions. Earth Planet. Sci. Lett. 333, 304-316.
678 Liu, S.-A., Teng, F.-Z., He, Y., Ke, S., Li, S., 2010. Investigation of magnesium isotope
679 fractionation during granite differentiation: Implication for Mg isotopic composition of
680 the continental crust. Earth Planet. Sci. Lett. 297, 646-654.
681 Marriott, C.S., Henderson, G.M., Belshaw, N.S., Tudhope, A.W., 2004. Temperature
682 dependence of delta Li-7, delta Ca-44 and Li/Ca during growth of calcium carbonate.
683 Earth Planet. Sci. Lett. 222, 615–624.
684 Milliman, J.D., 2010. Production and accumulation of calcium carbonate in the ocean: Budget
685 of a nonsteady state. Global Biogeoch. Cycl. 7, 927–957.
686 Nägler, T.F., Eisenhauer, A., Müller, A., Hemleben, C., Kramers, J., 2000. The $\delta^{44}Ca$
687 temperature calibration on fossil and cultured *Globigerinoides sacculifer*: new tool for
688 reconstruction of past sea surface temperatures. Geochem. Geophys. Geosyst. 1,
689 1052. doi:10.1029/2000GC000091.
690 Nogueira, A.C.R., Riccomini, C., Sial, A.N., Moura, C.A.V., Trindade, R., Fairchild, T.R.,
691 2007. Carbon and strontium isotope fluctuations and paleoceanographic changes in

692 the late Neoproterozoic Araras carbonate platform, southern Amazon craton, Brazil.
693 Chem. Geol. 237, 168-190.
694 Payne, J.L., Turchyn, A.V., Paytan, A., DePaolo, D.J., Lehrmann, D.J., Yu, M., Wei, J., 2010.
695 Calcium isotope constraints on the end-Permian mass extinction. Proc. Natl. Acad.
696 Sci. 107, 8543-8548.
697 Pierrehumbert, R.T., 2004. High levels of carbon dioxide necessary for the termination of
698 global glaciations. Nature 429, 646-649.
699 Pogge von Strandmann, P.A.E., Burton, K.W., James, R.H., van Calsteren, P., Gislason, S.
700 R., Sigfusson, B., 2008. The influence of weathering processes on riverine
701 magnesium isotopes in a basaltic terrain. Earth Planet. Sci. Lett. 276, 187-197.
702 Pogge von Strandmann, P.A.E., 2008. Precise Magnesium Isotope Measurements in Core-
703 top Planktic and Benthic Foraminifera. Geochem. Geophys. Geosyst. 9,
704 doi:10.1029/2008GC002209.
705 Pogge von Strandmann, P.A.E., Elliott, T., Marschall, H.R., Coath, C.D., Lai, Y.J., Jeffcoate,
706 A.B., Ionov D.A., 2011. Variations of Li and Mg isotope ratios in bulk chondrites and
707 mantle xenoliths. Geochim. Cosmochim. Acta 75, 5247-5268.
708 Pogge von Strandmann, P.A.E., Opfergelt, S., Lai, Y.J., Sigfusson, B., Gislason, S.R.,
709 Burton, K.W., 2012. Lithium, magnesium and silicon isotope behaviour accompanying
710 weathering in a basaltic soil and pore water profile in Iceland. Earth Planet. Sci. Lett.
711 339-340, 11-23.
712 Pogge von Strandmann, P.A.E., Jenkyns, H.C., Woodfine, R.G., 2013. Lithium isotope
713 evidence for enhanced weathering during Oceanic Anoxic Event 2. Nature
714 Geoscience 6, 668-672.
715 Pokrovsky, B.G., Mavromatis, V., Pokrovsky, O.S., 2011. Co-variation of Mg and C isotopes
716 in late Precambrian carbonates of the Siberian Platform: A new tool for tracing the
717 change in weathering regime? Chem. Geol. 290, 67-74.
718 Ridgwell, A.J., Kennedy, M.J., Caldeira, K., 2003. Carbonate deposition, climate stability, and
719 Neoproterozoic ice ages. Science 302, 859-862.

720 Shen, B., Jacobsen, B., Lee, C.-T.A., Yin, Q.-Z., Morton, D.M., 2009. The Mg isotopic
721 systematics of granitoids in continental arcs and implications for the role of chemical
722 weathering in crust formation. Proc. Natl. Acad. Sci. 106, 20652-20657.
723 Silva-Tamayo, J.C., Nägler, T.F., Villa, I.M., Kyser, K., Vieira, L.C., Sial, A.N., Narbonne,
724 G.M., James, N.P., 2010a. Global Ca isotope variations in ca. 0.7 Ga old postglacial
725 successions. Terra Nova, doi:10.1111/j.1365-3121.2010.00933.x.
726 Silva-Tamayo, J.C., Nägler, T.F., Sial, A.N., Nogueira, A., Kyser, K., Riccomini, C., James,
727 N.P., Narbonne, G.M., Villa, I.M., 2010b. Global perturbation of the marine Ca
728 isotopic composition in the aftermath of the Marinoan global glaciation. Precambrian
729 Research 182, 373-381.
730 Steuber, T., Buhl, D., 2006. Calcium-isotope fractionation in selected modern and ancient
731 marine carbonates. Geochim. Cosmochim. Acta 70, 5507-5521.
732 Tang, J., Dietzel, M., Böhm, F., Köhler, S.J., Eisenhauer, A., 2008. Sr^{2+}/Ca^{2+} and $^{44}Ca/^{40}Ca$
733 fractionation during inorganic calcite formation: II. Ca isotopes. Geochim.
734 Cosmochim. Acta 72, 3733-3745.
735 Tipper, E.T., Galy, A., Bickle, M.J., 2006a. Riverine evidence for a fractionated reservoir of
736 Ca and Mg on the continents: Implications for the oceanic Ca cycle. Earth Planet. Sci.
737 Lett. 247, 267-279.
738 Tipper, E.T., Galy, A., Gaillardet, J., Bickle, M.J., Elderfield, H., Carder, E.A., 2006b. The
739 magnesium isotope budget of the modern ocean: constraints from riverine
740 magnesium isotope ratios. Earth Planet. Sci. Lett. 250, 241-253.
741 Tipper, E.T., Gaillardet, J., Louvat, P., Capmas, F., White, A.F., 2010. Mg isotope constraints
742 on soil pore-fluid chemistry: Evidence from Santa Cruz, California. Geochim.
743 Cosmochim. Acta 74, 3883-3896.
744 Trindade, R.I.F., Font, E., D'Agrella-Filho, M.S., Nogueira, A.C.R., Riccomini, C., 2003. Low
745 latitude and multiple geomagnetic reversals in the Neoproterozoic Puga cap
746 carbonate, Amazon craton. Terra Nova 15, 441-446.

747 Walker, J.C.G., Hays, P.B., Kasting, J.F., 1981. A negative feedback mechanism for the
748 long-term stabilization of the Earth's surface temperature. J. Geophys. Res. 86, 9776-
749 9782.
750 Wilkinson, B.H., Algeo, T.J., 1989. Sedimentary carbonate record of calcium-magnesium
751 cycling. Am. J. Sci. 289, 1158-1194.
752 Williams, G.E., 1979. Sedimentology, stable-isotope geochemistry and palaeoenvironment of
753 dolostones capping late Precambrian glacial sequences in Australia. J. Geol. Soc.
754 Aust. 26, 377-386.
755 Zhu, P., Macdougall, J.D., 1998. Calcium isotopes in the marine environment and the
756 oceanic calcium cycle: Geochim. Cosmochim. Acta 62, 1691-1698.
757
758 **Fig. captions**
759 Fig. 1. Generalized geological map of northern Namibia showing location of three
760 Neoproterozoic carbonate sections (modified after Kasemann et al., 2010). See text for
761 discussion.
762
763 Fig. 2. Composite B, C, Mg and Ca isotope records for younger Cryogenian postglacial
764 carbonate sections in Namibia. Transect from deeper- to shallow-marine settings,
765 including(a) the Fransfontein section from the ridge shelf-slope break and the Ombaatje
766 section from the shallow shelf, as well as (b) the nearby shallow shelf Khowarib section.
767
768 Fig 3. Expanded (log-) view of the Mg and Ca isotope records for the younger Cryogenian
769 postglacial carbonate sections in Namibia.
770
771 Fig. 4. Ca isotope records of the Keilberg–Maieberg formations in NW Namibia and the
772 coeval post-glacial carbonate successions in Brazil and NW Canada from Silva-Tamayo et
773 al. (2010b).
774

775 Fig. 5. Schematic overview on the relative shift in Ca and Mg isotope composition in
776 carbonates as a function of factors that could have been present in the Neoproterozoic world.
777 *Changes in the isotope composition induced by the precipitation rate and mineralogy
778 (aragonite/calcite) are only valid for calcium. Changes in the Mg isotope ratio induced by
779 temperature have been so far only observed for carbonates precipitated under laboratory
780 conditions (see text for discussion).
781
782 Fig. 6. Crossplots of B, C, Mg and Ca isotope data for the postglacial carbonate rocks from
783 the Ombaatjie platform section. The arrows in (a) to (d) indicate the stratigraphic sequence of
784 samples from the base to the top of the postglacial section. The open circle represents the
785 basal Keilberg cap contact sample. The correlation coefficient r in (a) and (b) is given for the
786 postglacial rocks excluding the contact sample.
787
788 Fig. 7. Parameter values used in the oceanic box model. Model parameters are derived from
789 Blattler et al. (2011); DePaolo (2004); Higgins and Schrag (2010); Holland (2005); Milliman
790 (1993); Tipper et al. (2006a,b); Wilkinson and Algeo (1989). Initial river isotope ratios as well
791 as the Ca seawater reservoir were taken from modern with subsequent small adjustments to
792 achieve data-valid starting compositions. Seawater and output flux values respond to model
793 adjustments and changes over time.
794
795 Fig. 8. A combined plot of the dynamic box model outcome for the Mg and Ca isotope
796 excursion through time and the actual Mg and Ca isotope excursion (converted seawater
797 values) observed on the shelf-slope break (Fransfontein) and platform (Ombaatjie). The
798 model outcome for A and B is given for the weathering scenario proposed to best match the
799 Mg and Ca isotope excursion from slope to platform: a combined carbonate plus silicate
800 weathering flux respectively of 9 and 20 times present day for about 500 kyr, followed by a
801 dominant silicate weathering pulse of respectively 6 and 15 times present day for 1 Myr, as
802 well as high primary dolomite formation for the first e.g. 100 kyr (cap dolostone, 85% Mg

sink) followed by primary calcite formation. The arrows indicate the timing of the expected change in weathering regime. The relative position of the analysed Mg and Ca isotope data and Formation boundaries on the time axis is given by the stratigraphic sequence; assumed timescale and rate of deposition can only be regarded as mean values. Model C and D represent the outcome for an exclusive silicate weathering influx of 20x for 1 Myr and 5x for 1 Myr, respectively (see text for discussion).

Fig. 9. Composite boron, carbon, calcium and magnesium (B, C, Ca, Mg) isotope record together with palaeo-pH and continental weathering flux reconstructions for the post-Ghaub carbonate succession at Fransfontein (foreslope) in northern Namibia (modified after Kasemann et al., 2010). Grey area marks average B isotope composition and ocean pH conditions of inferred Neoproterozoic climatic normalcy. Arrow indicates inferred transient ocean acidification event. For a detailed discussion on the boron and pH data see Kasemann et al. (2010).

***Highlights (for review)**

Highlights

- We investigate Earth system response and recovery to extreme environmental conditions in the Neoproterozoic.
- Calcium and magnesium isotopes indicate an enhanced continental weathering flux after a global glaciation.
- Continental weathering enabled the ocean to recover from an ocean acidification state.

Figure_1

Click here to download high resolution image

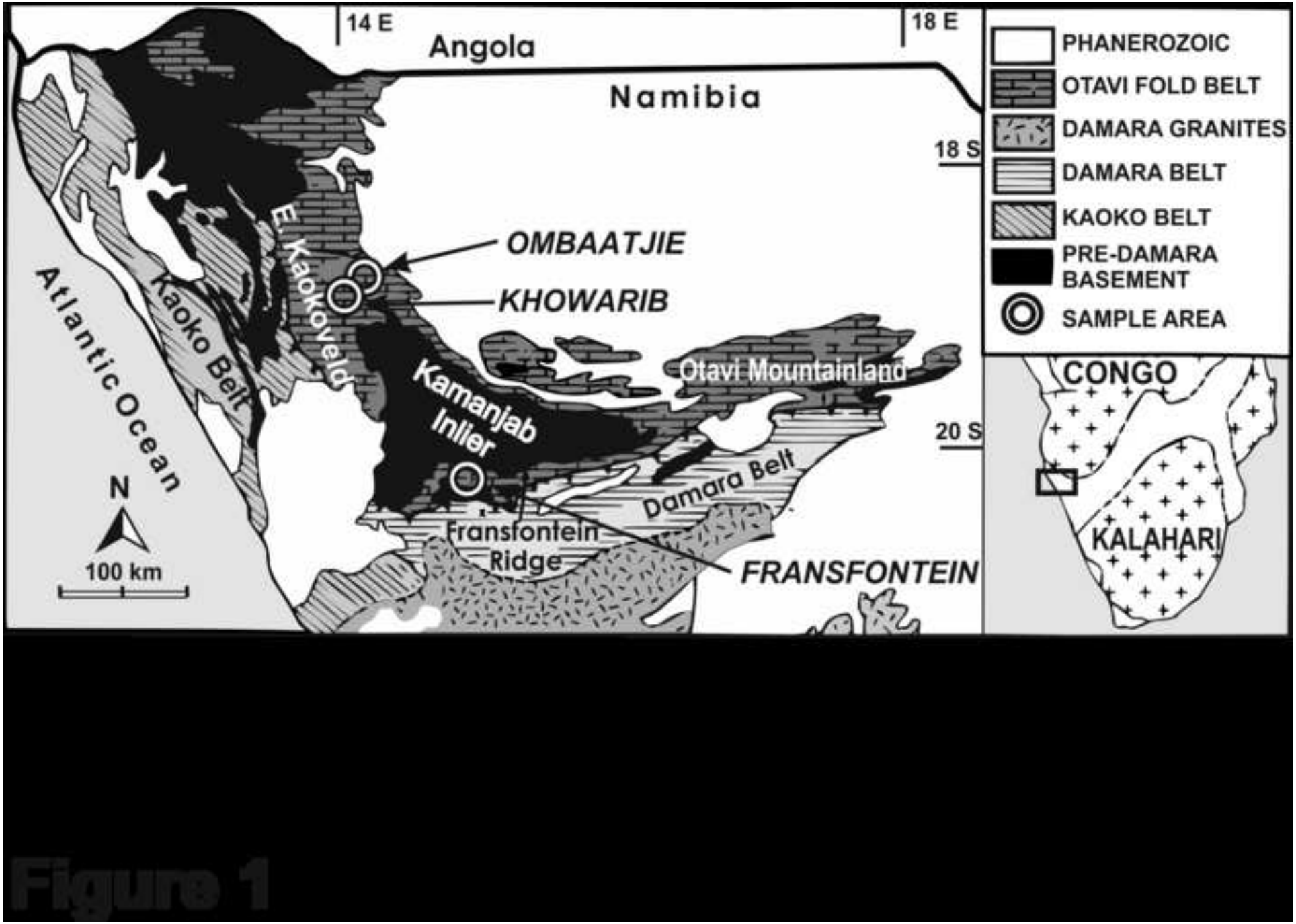

Figure_2

Click here to download high resolution image

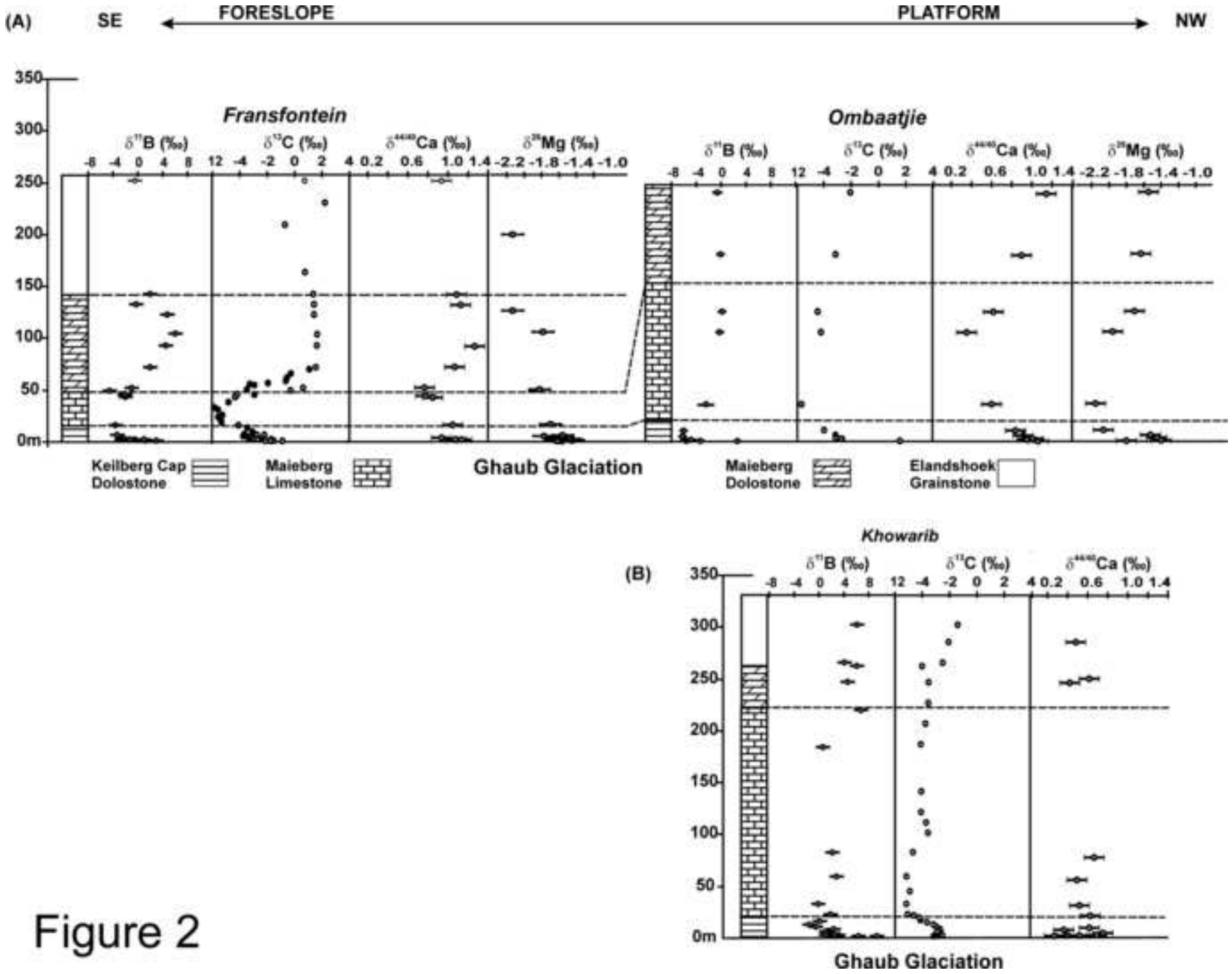

Figure 2

Figure_3
Click here to download high resolution image

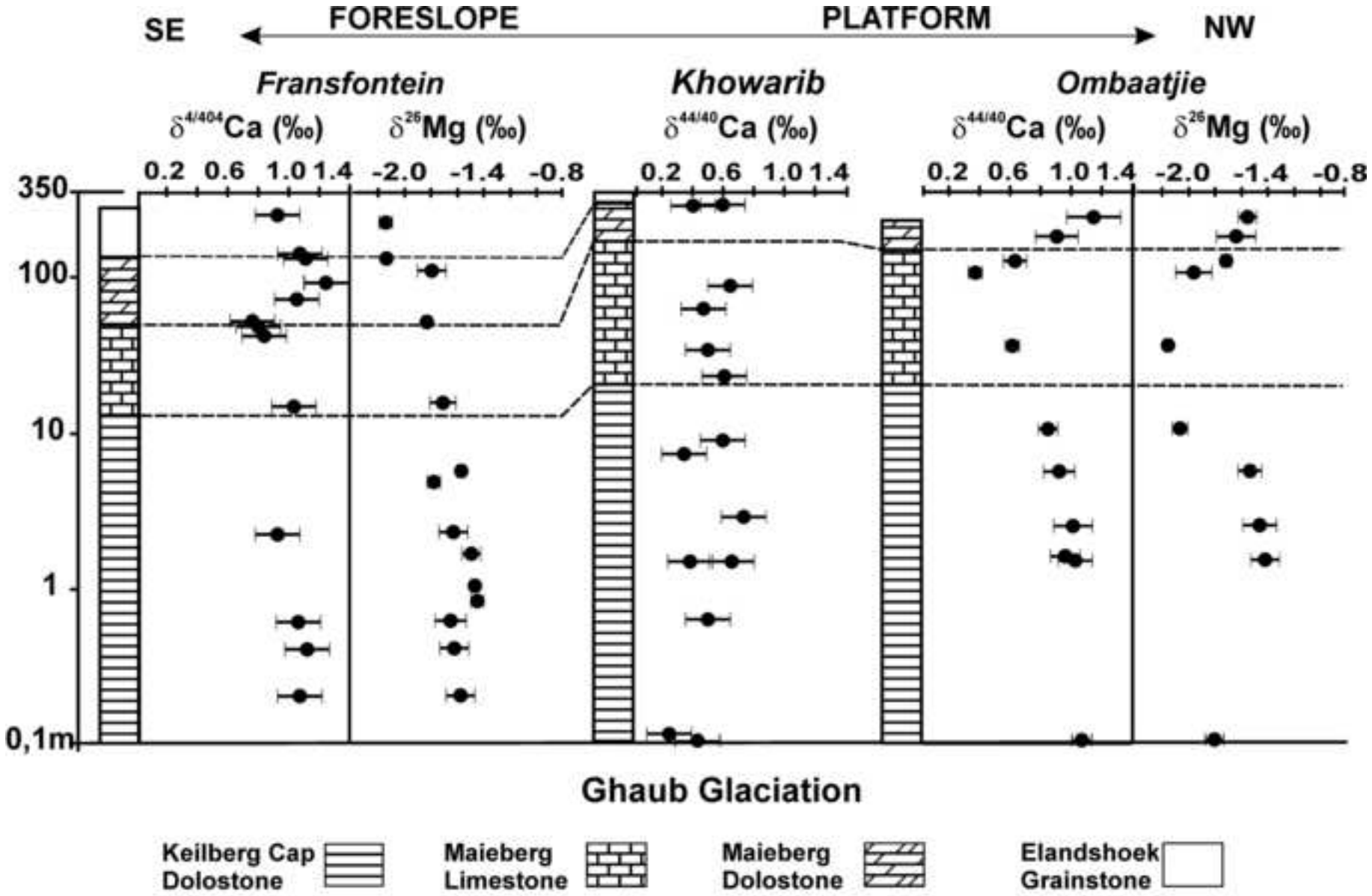

Figure 3

Figure_4
Click here to download high resolution image

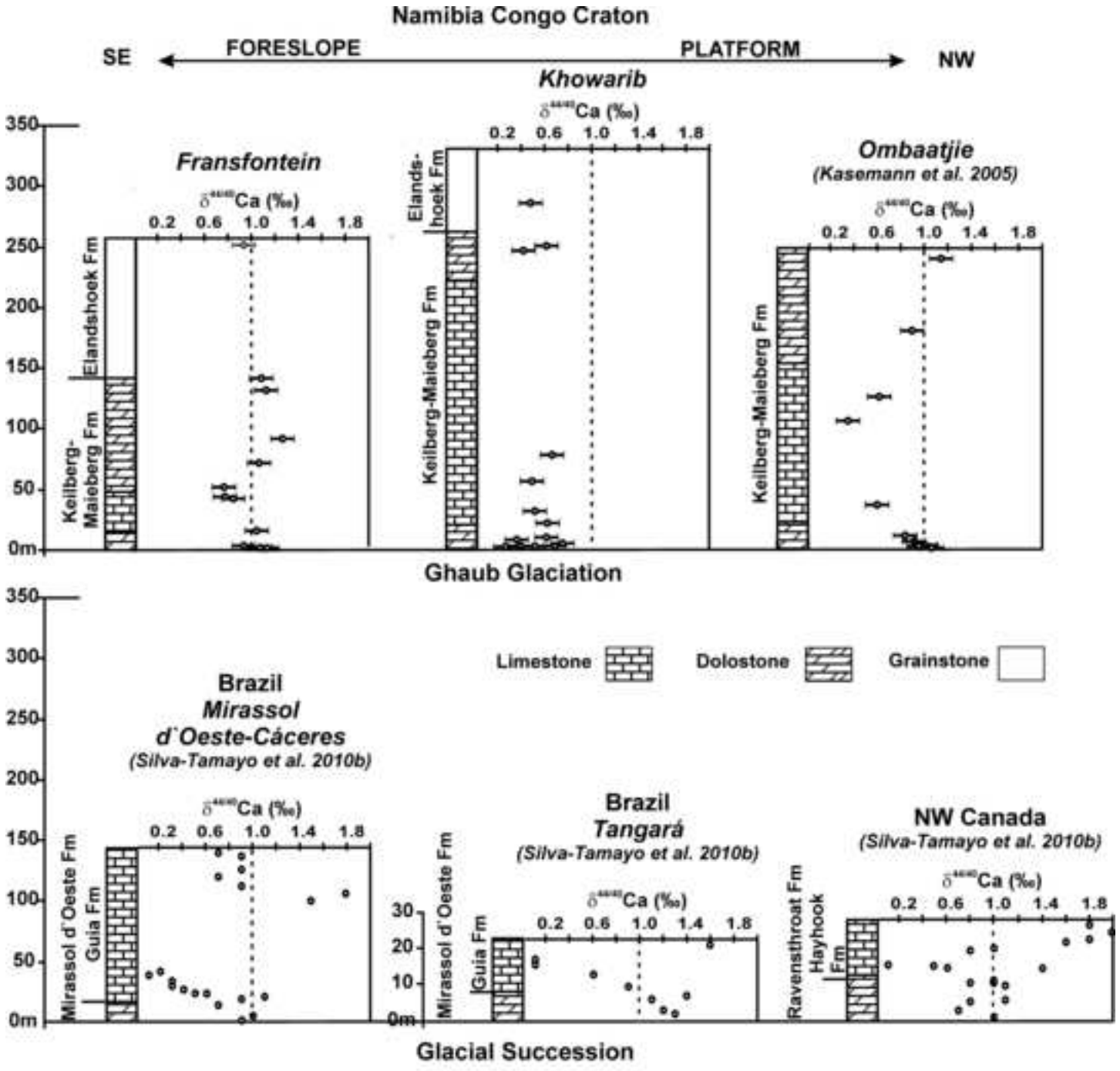

Figure 4

Figure_5
Click here to download high resolution image

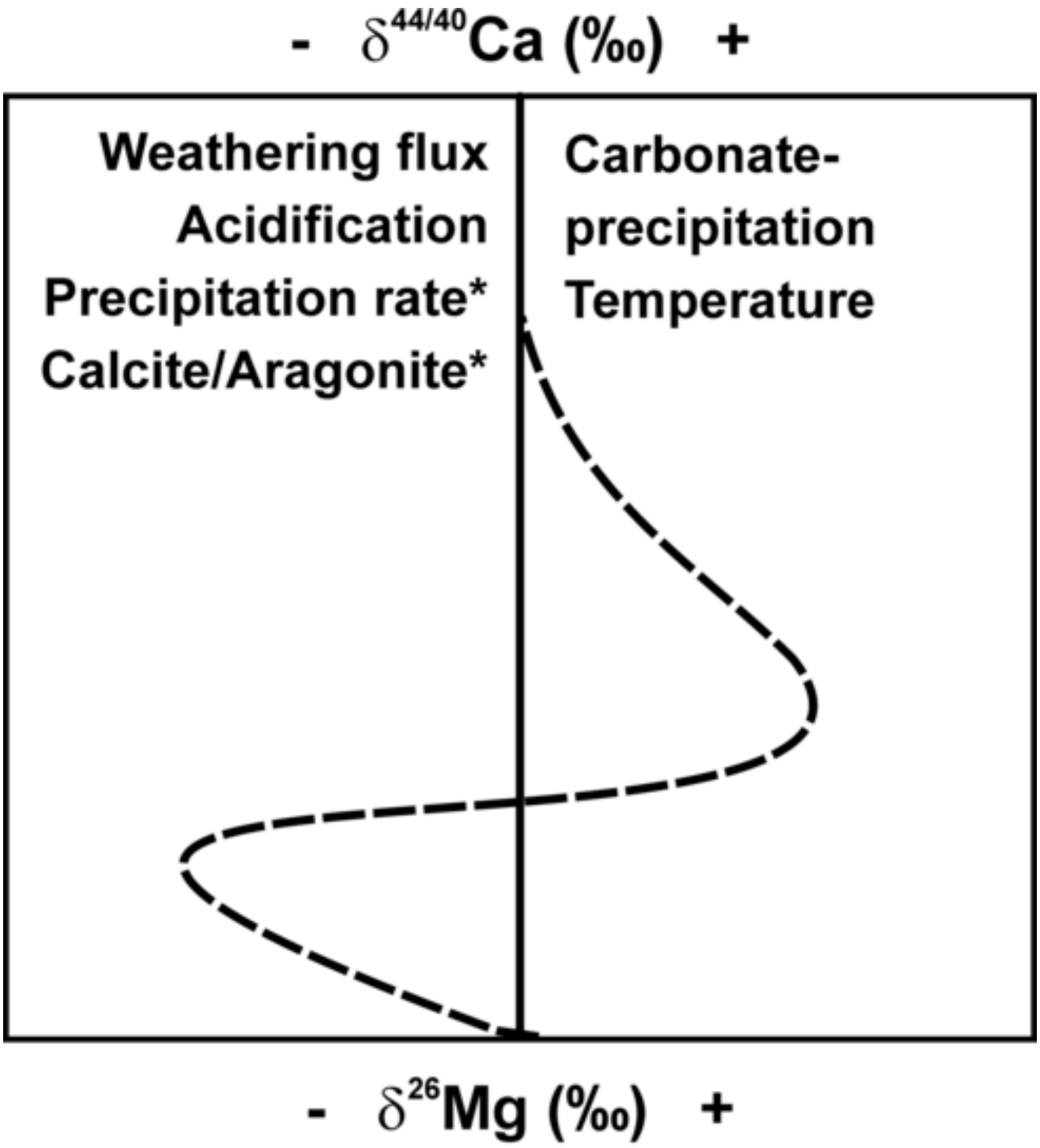

Figure 5

Figure_6
Click here to download high resolution image

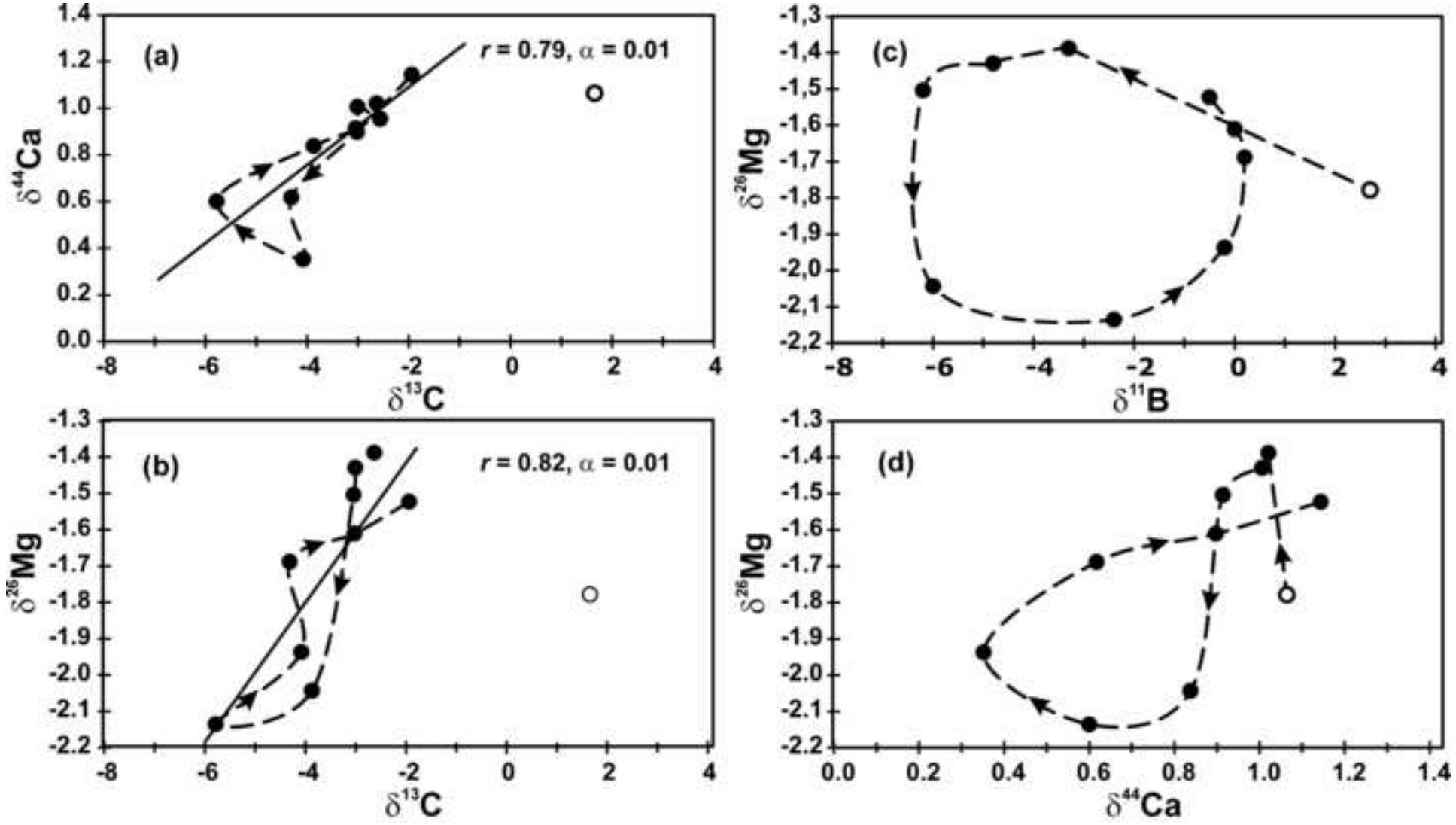

Figure 6

Figure_7
Click here to download high resolution image

Parameter	Ca: value and unit	Mg: value and unit
Initial		
River flux	2.3×10^{13} mol y^{-1}	5.6×10^{12} mol y^{-1}
River isotope composition	1.0 ‰	-1.0 ‰
Perturbed		
Isotope composition silicate flux endmember	1.2 ‰	-0.3 ‰
Isotope composition carbonate flux endmember	0.8 ‰	-2.5 ‰
$Seawater_{initial}$	1.4×10^{19} mol	7.3×10^{19} mol
Hydrothermal flux	2.0×10^{12} mol y^{-1}	
Hydrothermal isotope composition	0.9 ‰	
Carbonate precipitation $\Delta_{carb\text{-}aqueous}$	-0.8 ‰	-2.7 ‰

Figure 7

Figure_8
Click here to download high resolution image

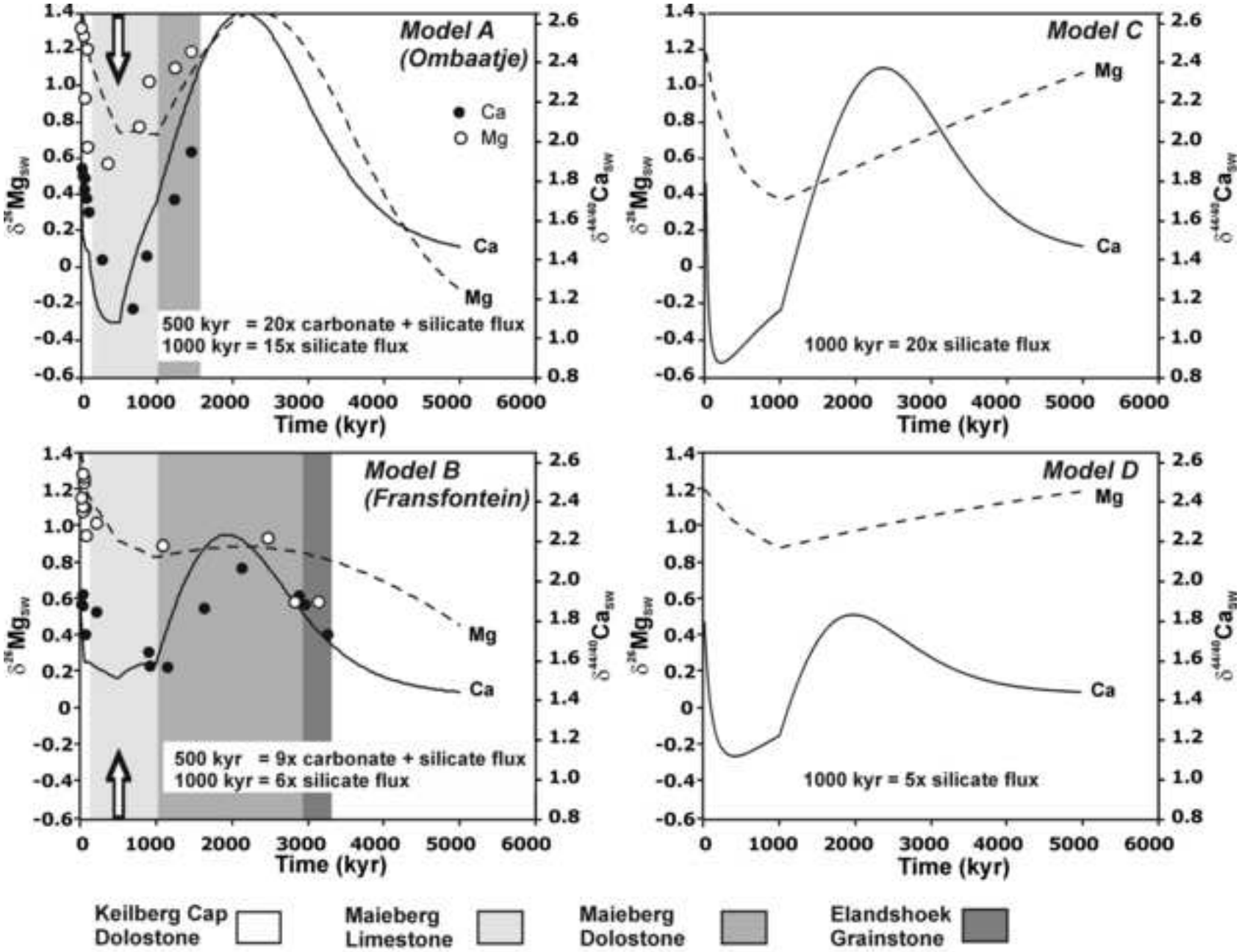

Figure 8

Figure_9
Click here to download high resolution image

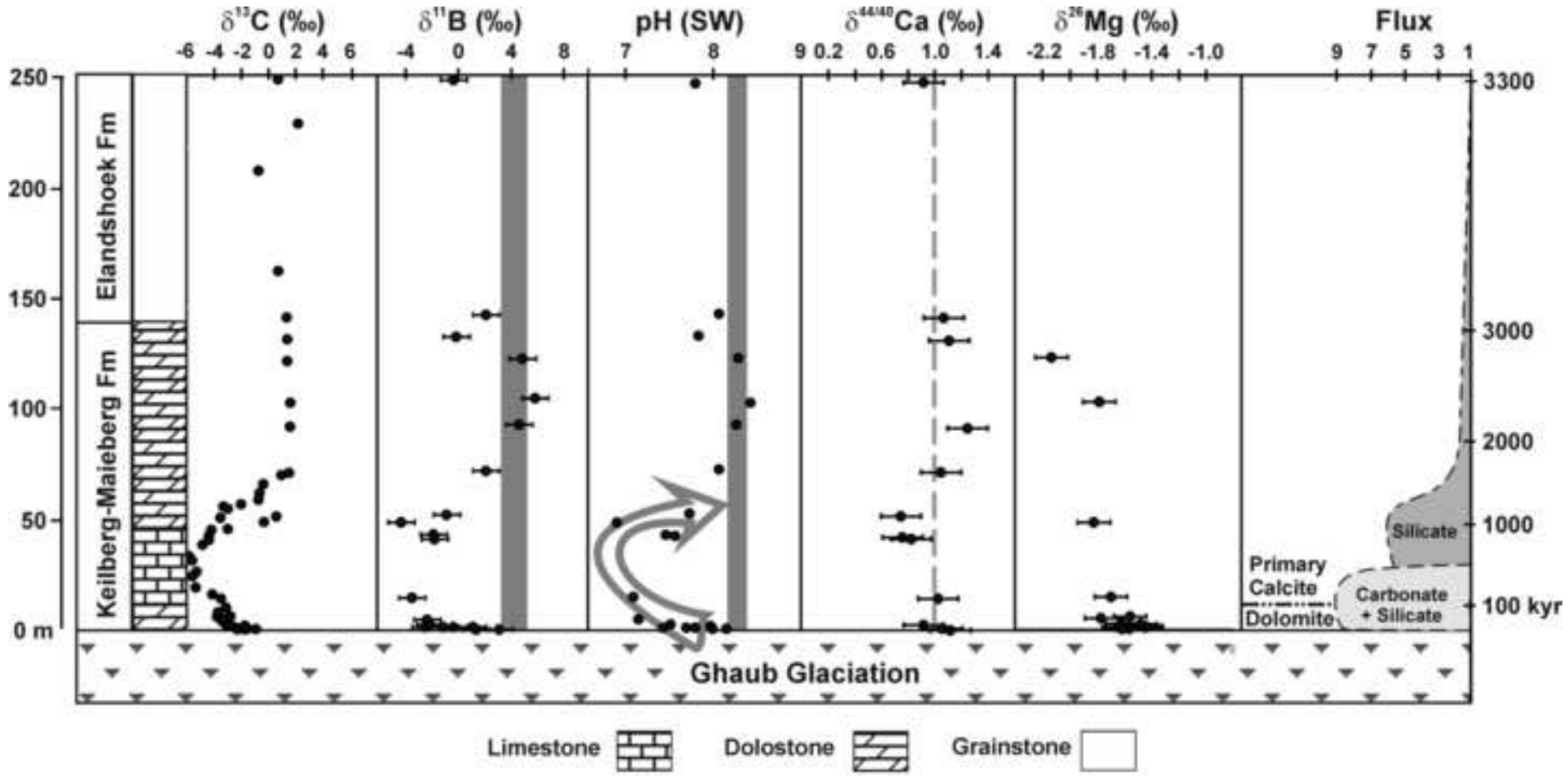

Figure 9

Supplementary material for on-line publication only

Click here to download Supplementary material for on-line publication only: Supporting_Online_Material_final.docx

Table S1

Click here to download Supplementary material for on-line publication only: Table_S1.xlsx